Final Report

Synthesis and cytotoxicity study of magnetic three-dimensionally ordered macroporous Fe-substituted hydroxyapatite (3DOM FeHAp)

By Supakit Achiwawanich

July 2018

Abstract

Project Code : TRG5780289

Project Title : Synthesis and cytotoxicity study of magnetic three-dimensionally ordered macroporous Fe-substituted hydroxyapatite (3DOM FeHAp)

Investigator : Supakit Achiwawanich **E-mail Address :** fsciska@ku.ac.th

Project Period : 2 years

Abstract:

Three dimensionally ordered macroporous (3DOM) hydroxyapatite (HAp) and iron substituted 3DOM HAp was successfully synthesized by sol-gel method using PMMA colloidal crystal arrays. The highest HAp phase of 77.0% was found in the 3DOM HAp after aging time of 10 hours and the maxima of 78.4% HAp was obtained in the 3DOM FeHAp 7%mol after aging time of 8 hours. Both synthesized HAp was characterized using X-ray diffraction spectrometry (XRD), Fourier transformed infrared spectroscopy (FTIR) and scanning electron microscopy (SEM). The 3DOM HAp and the 3DOM FeHAp 7%mol was paramagnetic whereas the 3DOM FeHAp 14-28% mol was superparamagnetic. The 3DOM FeHAp 28% mol exhibited the highest magnetization at 1.556 emu g^{-1}. Cytotoxicity study suggested that all samples were non-cytotoxic to osteoblasts. The study on drug delivery application of the 3DOM HAp and the 3DOM FeHAp were carried out using vancomycin as a drug model and the results were compared with that of the HAp derived from natural materials. Drug loading of vancomycin in the 3DOM HAp, the 3DOM FeHAp and the HAp from natural materials were 72.1%, 80.6%, and 33.1%, respectively. The percentage of cumulative vancomycin release were 72.1%, 80.6%, and 33.1% for the 3DOM HAp, the 3DOM FeHAp, and the HAp from natural materials, respectively.

Keywords: Iron, Hydroxyapatite, Three-dimensionally ordered macroporous material (3DOM)

Abstract:

Three dimensionally ordered macroporous (3DOM) hydroxyapatite (HAp) and iron substituted 3DOM HAp was successfully synthesized by sol-gel method using PMMA colloidal crystal arrays. The highest HAp phase of 77.0% was found in the 3DOM HAp after aging time of 10 hours and the maxima of 78.4% HAp was obtained in the 3DOM FeHAp 7%mol after aging time of 8 hours. Both synthesized HAp was characterized using X-ray diffraction spectrometry (XRD), Fourier transformed infrared spectroscopy (FTIR) and scanning electron microscopy (SEM). The 3DOM HAp and the 3DOM FeHAp 7%mol was paramagnetic whereas the 3DOM FeHAp 14-28% mol was superparamagnetic. The 3DOM FeHAp 28% mol exhibited the highest magnetization at 1.556 emu g^{-1}. Cytotoxicity study suggested that all samples were non-cytotoxic to osteoblasts. The study on drug delivery application of the 3DOM HAp and the 3DOM FeHAp were carried out using vancomycin as a drug model and the results were compared with that of the HAp derived from natural materials. Drug loading of vancomycin in the 3DOM HAp, the 3DOM FeHAp and the HAp from natural materials were 72.1%, 80.6%, and 33.1%, respectively. The percentage of cumulative vancomycin release were 72.1%, 80.6%, and 33.1% for the 3DOM HAp, the 3DOM FeHAp, and the HAp from natural materials, respectively.

Keywords: Iron, Hydroxyapatite, Three-dimensionally ordered macroporous material (3DOM)

Introduction

One of the most important minerals in the apatite group is hydroxyapatite, $Ca_{10}(PO_4)_6(OH)_2$, an inorganic material analogous to the major components in bones. Attributed to its biocompatibility; osteoconductivity and osteoinductivity, hydroxyapatite (HAp) has been attracted great interest as an orthopedic implant replacement and drug delivery agent. However, the medical applications of HAp are restricted because of its poor mechanical properties [1, 2]. Therefore, it is necessary to improve the HAp mechanical properties. One of the several approaches is chemical modification or ion-substituted HAp which could increase mechanical strength and also bioactivity of the synthetic HAp since some ions may play an important role for in the growth of artificial bone [3, 4], for example, Si-substituted HAp increase cell proliferation when compared with pure HAp [5].

Iron (Fe) is a trace element commonly found in bones and teeth and is also known to have an effect on calcium phosphates, a HAp precursor, crystallization [6]. Furthermore, by incorporating Fe into HAp, not only enhance the mechanical property of the HAp but also promote magnetism to the HAp material. This biomagnetised material have received great attentions because of their extended medical applications including being used as a contrast agent for magnetic resonance imaging, hyperthermia treatment for cancer and magnetic targeting drug delivery [7, 8]. Although study on the role of Fe-doped HAp as a biomaterial is limited, there are few researches shown that FeHAp is significantly increase in cell proliferation and higher osteoblast activity [9] with prolonged antibiotic and anticancer drug release [10].

Over the last few years, many studies have been developed to fabricated new material structure using periodic colloidal polymeric templates, allowing them to achieve three-dimensionally ordered macroporous (3DOM) materials [11, 12]. This approach

employs monodispersed spherical polymer to self-assemble into close-packed array, creating an opal arrangement [13]. The interstitial voids between the polymeric spheres are then infiltrated with a fluid or a precursor solution which become solid wall of 3DOM materials after calcination. The original polymeric spheres are removed resulting in interconnected void (Fig. 1). These 3DOM materials offer diverse benefits over other porous materials derived from less regular templating methods. The highly ordered materials provide three-dimensional hierarchical structure, relatively large surface areas and facile transportation of molecules through the entire surface.

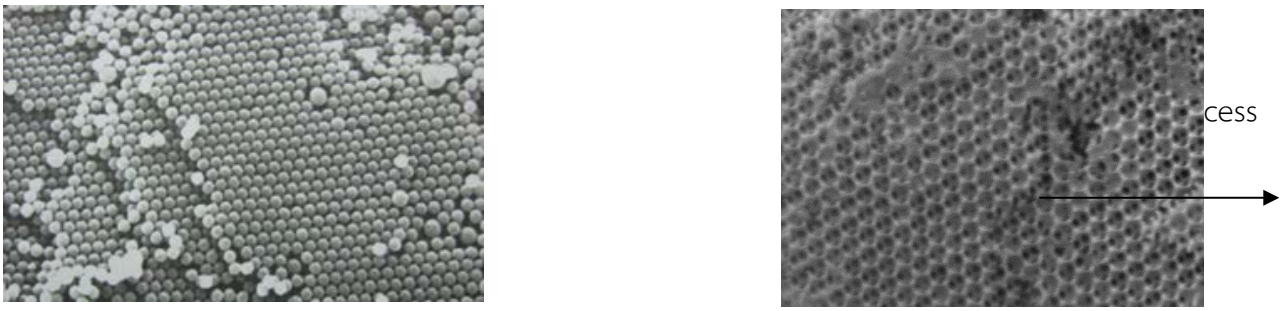

Figure 1 SEM images of a close-packed polymeric template and 3DOM HAp [14].

Although syntheses and applications of HAp or FeHAp have been studied [9, 10, 15-21], few publications on macroporous materials, especially the 3DOM FeHAp, are reported. In this research, we incorporate the concepts of sol-gel synthesis and self-assembled colloidal polymeric templating technique to fabricate three-dimensionally ordered macroporous Fe-substituted hydroxyapatite (3DOM FeHAp). The research is sought to produce, characterize the synthesized 3DOM FeHAp and further investigate the cytotoxicity of the FeHAp on live cells. With highly ordered porosity with network of macropores and more accessible surface of this synthetic 3DOM FeHAp may allow

possibility of faster growth of apatite and greater drug uptake than mesoporous and nanoporous biomaterials [22-25]. Moreover, the magnetic property of the 3DOM FeHAp will be investigated. Positive results may extend its applications towards anticancer therapy based on hyperthermia.

Literature review

Colloidal polymeric templating method

Opals, one of the most colourful gemstones, are composed of primarily silicon and oxygen in a form of SiO_2. Typical pure silica is colourless, however, opals exhibit unique phenomena, called "play of colour", displaying rainbows colour. This phenomenon, often known as opalescence, is caused by ordered microscopic closest packed arrangement of SiO_2 spheres. When light travels to surface of opals, it reflects resulting in diffraction of light from the SiO_2 plane. Because the diameter of silica spheres are in hundred of nanometer, the lights can be diffracted when traveling through the silica spheres resulting in the flashes of colour.

Since an achievement of synthesis of monodispersed polymeric spheres [26-29], it has attracted researchers to developed periodic framework materials by mimicking the opal's arrangement. This highly ordered arrangement of the monodispersed latex is accomplished by centrifugation, sedimentation and electrophoresis. The discovery of the self-assembling system leads to an attention to employ this arrangement as templates for nano-, meso-, and macroporous structure materials fabrications. Metals, Inorganic sulfides, oxides, carbon and polymers have been templated or fabricated using this method, resulting in periodic porous materials those show great properties in photonics, sensing and electronic applications [11, 12, 30-32].

Hydroxyapatite

Apatite is one of significant minerals for mineralogist, biologists and inorganic chemists owing to its chemical constituents similar to bone and hard tissues in mammal. The chemical composition of apatite may be written as $M_{10}(ZO_4)_6X_2$ where M, Z and X sites may be substituted by many chemical constituents.

Hydroxyapatite (HAp), is a naturally occurring mineral in a form of calcium apatite with a formula of $Ca_5(PO_4)_3(OH)$, however, it is usually written as $Ca_{10}(PO_4)_6(OH)_2$ to emphasize the crystal unit cell. Its unit cell contains a complete representation of the apatite crystal, consisting of Ca^{2+}, PO_4^{3-}, and OH^- with the Ca/P molar ratio in the range of 1.5-1.67. HAp crystallizes in the hexagonal crystal system with the space group of $P6_3/m$. This space group is characterized by a six fold *c*-axis perpendicular to three equivalents *a*-axis (a_1, a_2, and a_3) at angle of 120°C to each other. The crystal structure and crystallographic data of HAp is shown in Fig. 2 and Table 1, respectively.

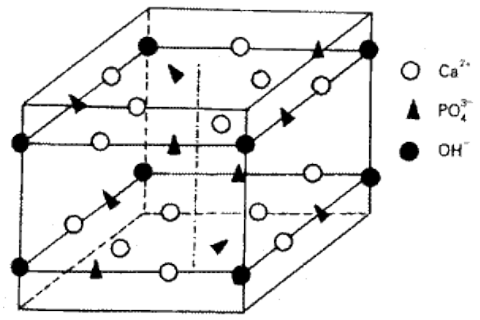

Figure 2 Hydroxyapatite unit cell [33].

Table 1 The crystallographic data of HAp [33]:

Crystal system	Hexagonal
Space group	$P6_3/m$
Lattice constants	a = 0.9432 c = 0.6881
Chemical unit number	Z=1
Specific gravity	3.08

The apatite structure is very hospitable in allowing the substitutions of many other ions into Ca^{2+}, PO_4^{3-}, and OH^- groups. The substitutions may cause morphological changes as well as their properties. For example, fluorapatite or fluoroapatite, a dental material, may be produced by ion substitution of OH^- ions by F^- ions causing shorten of a-axis [34].

Synthesis of hydroxyapatite via sol-gel method

Hydroxyapatite (HAp) can be synthesized using sol-gel method. The advantage of this method is that many forms and morphologies of HAp can be achieved by varying chemical precursors. The range of precursors include; calcium acetate and calcium chloride as Ca precursors and diammonium hydrogen phosphate $(NH_4)_2HPO_4$ or phosphoric pentoxide (P_2O_5) as P precursors. Moreover, addition of different surfactant such as cetyltrimethylammonium bromide (CTAB), sodium dodecyl sulfate (SDS) and polyoxyethylene cetyl ether (Brij56) can be used as a secondary template to enhance porosity of HAp.

Kuriakose *et al.,* [35] synthesized nanocrystalline HAp using calcium nitrate tetrahydrate and $(NH_4)_2HPO_4$ as starting calcium and phosphorous source. By using ethanol as a solvent under alkaline condition at 85°C, pure porous HAp was obtained after calcination at 1200°C. It was found that the presence of alcohol provide a thermally stable of the produced HAp. The presence of the pores may enhance it biocompatibility of HAp as they could enhance the adhesion between the natural and synthesized bone apatite. In 2004, Han *et al*. [36] reported the synthesis of nanocrystalline hydroxyapatite powder using the same precursors as used in Kuriakose *et al. ,* (2004) [35], however, Han *et al*. also added citric acid as an organic modifier. As a result, homogeneous HAp with higher surface area was obtained. The particle size of the HAp powder is between 80 and 150 nm with approximate porosity of 19 % and flexural strength of 37 MPa. Apart from citric acid as organic modifier, polyethylene glycol were also used to control particle size of synthesized HAp [37]. By employing this sol-gel synthesis chemical route, plate-like HAp crystals were obtained. The authors concluded that polyethylene glycol molecules induced the orientation growth which leads to the formation of HAP platelets with an average size of 50–70 nm.

Hydroxyapatite applications

HAp has been studied extensively in different medical applications such as drug delivery and bone replacement. Furthermore, it has also been studied for non-medical application, for example, as packing media for column chromatography, gas sensors, catalysts and adsorption metal in solution.

Fang *et al*. [38] studied HAp reinforced ultrahigh molecular weight polyethylene (UHMWPE) for biomedical applications. The processing method of combining ball milling and swelling was developed for HAp bio-composite. This method enhanced chain mobility

as a result of an interpenetrative network. The results showed that 90% increase in Young's modulus and 50% increase in the yield strength for the HAp bio-composite, comparing with unfilled UHMWPE.

Removal of toxic metals from waste water is also other applications of HAp [39]. An adsorption of Cd(II) and Cu(II) from aqueous solution by carbonate hydroxyapatite (CHAp) has been investigated by varying parameters such as contact time, solution pH, amount of CHAp and concentration of metal ions for maximum adsorption. The removal efficiency of Cd(II) and Cu(II) was 94% and 93.17%, respectively. Removal of lead(II) from aqueous solution was also studied [40], giving 101 mg/g of Pb(II) adsorption onto CHAP at pH 6.0.

Several studies have reported drug impregnation and release on mesoporous hydroxyapatite using ibuprofen [41], norfloxacin [22], and also vascular endothelial growth factor (VEGF) [42]. Results from *In vitro* studies showed that HAp may be a potential biomaterial for controlled releasing medium in medical applications. The cytotoxicity and apoptosis-induction of HAp nanoparticles have been discovered its cytotoxicity and apoptosis-induction of HAp nanoparticle using HepG2 cells were investigated [43]. It was found that the size of HAp affected the cellular uptake and nuclear localization in HepG2 cells.

Iron-substituted hydroxyapatite (FeHAp)

It has been known that biological and chemical properties of HAp may be altered by incorporation of impurities into its structure. Ming *et al.,* [44] studied only on local geometry of Fe^{2+}/Fe^{3+} in the FeHAp synthesized from precipitation of $Ca(NO_3)_2$, $Fe(NO_3)_2$ solution with $(NH_4)_2HPO_4$ using electron paramagnetic resonance, Mössbauer spectroscopy and electronic structure calculations. Anna, *et al*. [15] reported that superparamagnetic-

like behavior of the FeHAp with its biocompatibility on osteoblasts similar to that of pure HAp, making the FeHAp a potential material that can be manipulated by external magnetic field.

Three-dimensionally ordered macroporous bioactive materials (3DOM materials)

3DOM structure and its interconnected macropores may facilitate mass transport that involved many applications such as catalysis, sorption, separation and surface activity because of its accessible surface. The 3DOM HAp was used to capture heavy metals, including cadmium and lead, giving excellent sorption ability over HAp powder [45]. In the field of bioactive materials, several studies were focusing 3DOM bioactive glass [23-25, 46] with promising results over conventional bioactive glass. With hierarchical structure and high porosity of the 3DOM bioactive glass, these features accelerate growth of apatite with no cytotoxicity. Recently, a study of the 3DOM HAp as antibiotic drug carrier showed that the amount of loading drug were greater when compared with that of HAp derived from natural materials [14].

Objectives

1) To synthesized the 3DOM HAp and the 3DOM FeHAp by sol-gel method using polymeric colloidal arrays as templates.

2) To investigate of morphology, phase compositions and structure of the 3DOM FeHAp produced by sol-gel synthesis and its magnetic property.

3) To investigate the cytotoxicity of the 3DOM FeHAp.

Methodology

Experimental procedure could be summarized in Scheme 1**.**

Scheme 1 Methodology overview

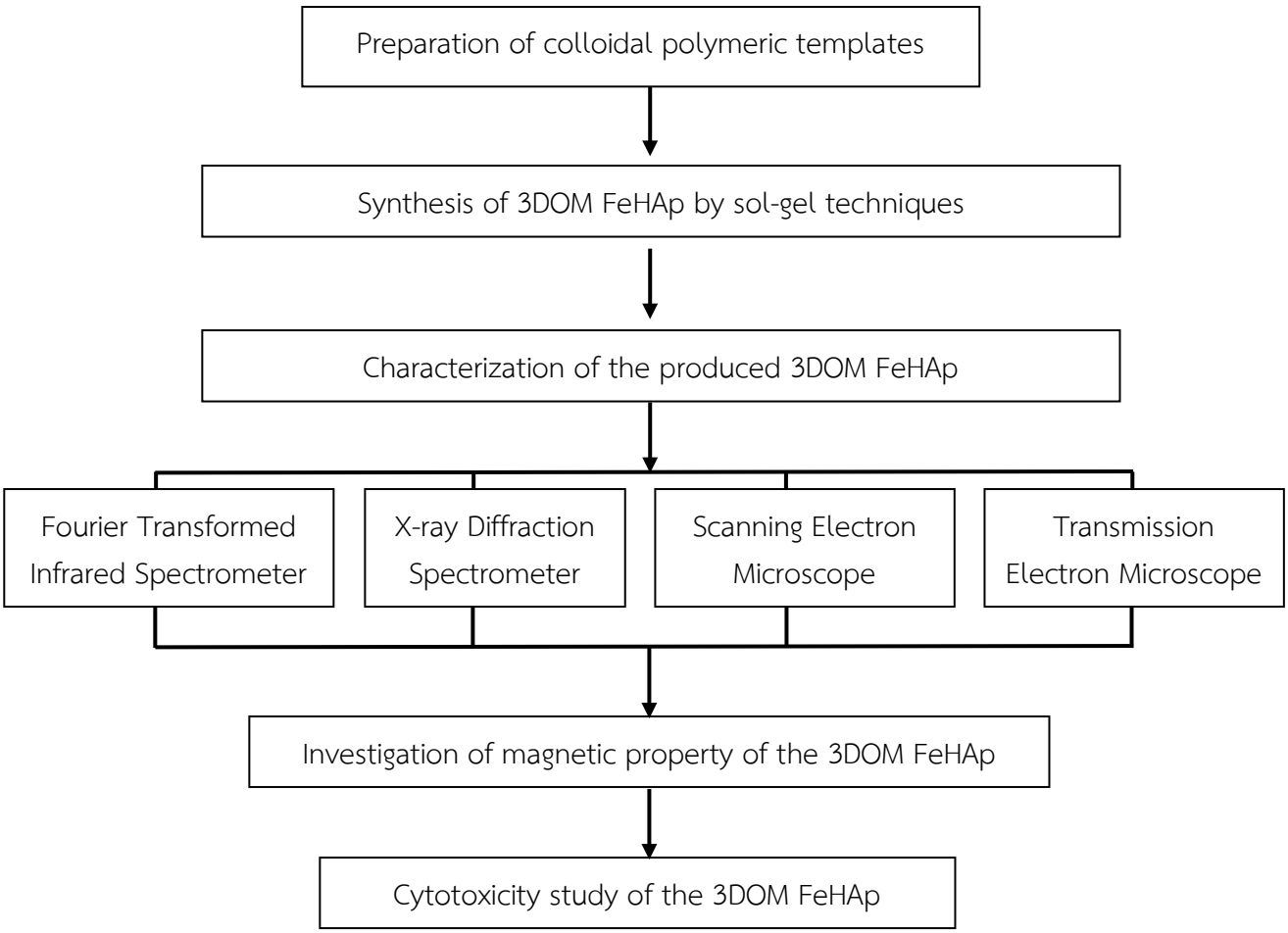

1. Preparation of monodispersed PMMA spheres: A polymeric colloidal templates for the 3DOM material fabrication

Preparation of monodispersed PMMA spheres was slightly adapted from the previous study by Schroden *et al.* [32]. Briefly, an emulsifier free emulsion polymerization

of methyl methacrylate (MMA) in water using 2,2'-Azobis(2-methylpropionamidine) dihydrochloride (AAPH) as an initiator was successfully synthesized was carried out at a constant temperature of 70 $^{\circ}$C for 2 hours [14], resulting in a PMMA colloidal suspension. After gravimetric sedimentation of the colloidal suspension, the polymeric colloidal templates could be achieved.

2. Sol-gel synthesis of the 3DOM HAp and the 3DOM FeHAp using polymeric colloidal arrays as templates

The synthesis of the 3DOM HAp has been previously described by Nitchakan [14]. Calcium nitrate tetrahydrate ($Ca(NO_3)_2.4H_2O$) and phosphorous pentoxide; (P_2O_5) in ethanol are used as Ca and P precursor for the HAp synthesis via sol-gel technique. A stoichiometric ratio of Ca/P is kept at 1.67. The P precursor solution was added dropwise into the Ca precursor. After vigorous stirring, a homogeneous HAp sol was infiltrated into the void of the polymeric templates with different aging time of 2, 4, 6, 8 and 10 hours. The infiltrated arrays were allowed to dry at room temperature for several days and then was subjected to calcination at 700 $^{\circ}$C for 3 hours in order to remove the polymeric templates, giving rise the 3DOM HAp (see Fig. 3).

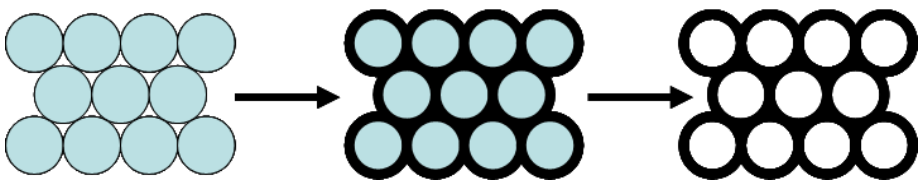

Figure 3. Typical fabrication process of 3DOM materials: a) polymeric colloidal arrays with closest packed arrangement, b) the polymeric template after infiltration with "sol" and c) 3DOM materials after calcination

The 3DOM FeHAp was prepared using the similar procedure to the 3DOM HAp synthesis. The solution of $Fe(NO_3)_2$ was added during the HAp sol preparation. The concentration of Fe was varied from 10-40 %.

3. Characterization of the synthesized 3DOM HAp and the 3DOM FeHAp

The as-synthesized 3DOM HAp and 3DOM FeHAp were characterized by FTIR, XRD, SEM and TEM techniques. The chemical functional groups of the 3DOM HAp and the 3DOM FeHAp were investigated by Equinox55 FTIR spectrophotometer (Bruker) in the range of 4000-400 cm^{-1} with resolution of 2 cm^{-1}. Surface morphology of both synthesized 3DOM HAp were examined by JSM 6310F Scanning Electron Microscope, JEOL. The phase composition and structure of the 3DOM HAp and the 3DOM FeHAp data were studied using D8 advance X-ray diffractometer. The intensity data was collected in the 2θ range of 5° to 80°, using a monochromatic Cu Kα radiation (λ = 1.54 Å). The scan rate was set at 1.5 step/2θ with the step of 0.02°. The phase composition was identified by comparison with the standard XRD patterns from the Joint Committee on Powder Diffraction Standards (JCPDS). The concentrations of Ca, P and Fe elements of the synthesized 3DOM materials were quantified by Optima 4300 DV ICP-OES at The Gem and Jewelry Institute of Thailand.

N_2 adsorption-desorption isotherms were measured be Micrometrics ASAP 2020 instrument. The powder samples were dried in a sample holder at 250°C in N_2 atmosphere for 12 hours. The Surface area analysis was carried out using five-point Brunauer Emmett and Teller surface area analysis (BET). The pore size distribution was determined from the adsorption branches of the isotherms by using the Barrelt-Joyner-Halenda method (BJH).

The magnetic property of the 3DOM HAp and the 3DOM FeHAp powder was studied using in-house vibrating sample magnetometer, at Physics Department, Faculty of Science, Kasetsart University.

4) Cytotoxicity study of the 3DOM HAp and the 3DOM FeHAp

4.1) Cell cuture

Osteoblast-liked cell (MC3T3-E1) from ATCC (ATCC® CRL-2593™) was maintained in 75 ml cell culture flasks containing alpha Minimum Essential Medium (α-MEM), supplemented with 10% fetal bovine serum (FBS) under a 5% CO_2 humidified atmosphere at 37 °C. The cell were allowed to grow upto 70-80% confluency. The cells were then rinsed twice with 1 ml of PBS buffer followed by incubation with 1ml of trypsin. After the cells were detached from the flask, they were resuspended in supplemented medium and replated onto new cell culture flasks. Cells were passaged once a week and passages 4-8 times before being used.

The number of viable cells in multi-well plates were determined by the *3-(*4,5-Dimethylthiazol-2-yl)-*5(*3-carboxymethonyphenol)-2-*(4*-sulfophenyl)-2H-tetrazolium or MTS assay. The assay works on the principle that mitochondria in viable cells reduce MTS resulting in a water-soluble coloured formazan product (Fig. 4). The absorbance of the formazan were recorded at 490 nm. This assay is used to quantify the living cell [47].

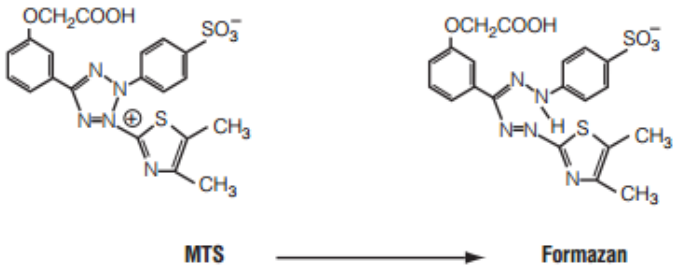

Figure 4. Structures of MTS tetrazolium and its formazan product.

4.2) Cell viability assay

The 3DOM HAp and the 3DOM FeHAp were steriled at 180 °C. The 3DOM materials were then immersed in α-MEM supplemented with 10% FBS and incubated at 37°C. The medium was collected for cell viability test. This extracted medium may contained leachable substances from the 3DOM samples which may cause toxicity to the living cells. In this study, the extraction medium was incubated with the 3DOM HAp materials at 2000 μg/ml, 1000 μg/ml, 500 μg/ml and 250 μg/ at 37 °C for 48 hours. The cultured cell was seeded into 96-well plates at a density of 8×10^{3} cell/well and incubated for 24 hours. The medium in each well was then replaced with the extraction medium and incubated for another 24 hours. The cultured cells in α-MEM and 10% FBS media were use as control. After 24 hours, 10 μl of MTS solution was added to each well and incubated for another 3 hours. The absorbance was measured by the Multiwell Scanning Spectrophotometer (ELISA reader) at 490 nm. The percentage of cell viability was calculated as follows:

$$\% \text{ viability} = \frac{\text{absorbance of treated cell}}{\text{absorbance of non untreated cell}} * 100 \qquad \text{(eq 1)}$$

4.3) Cell attachment

The cell attachment study was performed using standard protocol by Chen, C.S., et al., 2003. [48]. The 3DOM HAp and the 3DOM FeHAp powder embedded on resin composite were cut into small size and sterilized in an oven at 180 °C for 3 hours and then cultured in 96-well tissue-culture test plates. Subsequently, cells were seeded on the sterilized 3DOM materials at a density of 8×10^{3} cells/well and cultured for up to 24 hours. The samples were then transferred to new 96-well tissue-culture plates. For immono-fluorescence staining, the cells were removed from the 96-well tissue-culture plates, then washed with PBS and fixed with 4% paraformaldehyde for 20 minutes. The cells were rinsed twice with PBS and permeabilized cells with freshly prepared 0.1% triton X-100 in PBS for 10 minute. The cells were rinsed with PBS and incubated overnight with mouse anti-tubulin *(*1:100 in mg/ml bovine serum albumin, BSA/ PBS 4 $^{\circ}$C*)*. After that, the cells were washed in PBS three times and incubated with antibody at reaction time for 1 hour in dark room. Then, the cell were washed in 1% BSA, followed by 10% FBS in PBS and incubate with Hoechst dye (1:2500 in 1% BSA, 10% FBS in PBS) at room temperature for 1 hours. The cells were washed twice with PBS solution. Fluorescence microscope was employed to observed cell attachment.

5) Study of antibiotic drug carrier property of 3DOM HAp and 3DOM FeHAp using vancomycin as a drug model

5.1) Preparation of simulated body fluid *(*SBF*)*

SBF is a solution, which essential ion concentrations are similar to those in human blood plasma. The preparation of SBF in this study was prepared following the procedure

given by Kokubo and Takadama, 2006 [49]. The SBF preparation procedure was described herein.

1. The chemical 1st to 8th were dissolved in 700 ml of deionized water, respectively (Table 2). It is noted that each chemical must be completely dissolved before adding the next reagent.

2. Before adding the 9th reagent *(*Tris*)*, the volume of SBF solution must be over 900 ml, otherwise, the deionized water should be added. The pH of the solution now should be in the range of 1-3. Carefully adding Tris until the pH of SBF is less than 7.45. If the pH is more than 7.45, 1M HCl must be added to lower the pH to 7.42. The pH of the solution is adjusted by adding 1M HCl until pH 7.40 is obtained.

3. Finally, the total volume of SBF should be adjusted to 1000 ml by deionized water. The SBF solution must be kept in the plastic bottle at 5-10 °C.

Table 2 The reagents for SBF preparation.

Order reagent	Amount
1. NaCl	7.9962 g
2. $NaHCO_3$	0.3508 g
3. KCl	0.2246 g
4. K_2HPO_4	0.1744 g
5. $MgCl_2.6H_2O$	0.3069 g
6. 1M HCl	40 ml
7. $CaCl_2.2H_2O$	0.3694 g
8. Na_2SO_4	0.0712 g
9. $(CH_2OH)_3CNH_2$ *(*Tris*)*	5.7018 g

5.2) In vitro antibiotic drug delivery.

An antibiotic drug, vancomycin, was used as the drug model for drug delivery study using the synthesized 3DOM HAp and 3DOM FeHAp as drug carrier. The study of antibiotic drug carrier began with loading vancomycin into 3DOM HAp and 3DOM FeHAp compared with HAp derived from natural materials by Phumthiean, 2013 [14]. The concentrations of drug in the solution before and after loading were estimated spectrophotometrically at a wavelength of 281 nm. The percentages of drug loading per weight of the 3DOM HAp and 3DOM FeHAp were calculated as shown in Eq 2.

$$\% \ drug \ \ loading \ = \ \frac{\frac{x-y}{x} * 100}{\text{grams of HAp}} \qquad \text{(eq 2)}$$

: x and y = the initial and final weight of drug, respectively.

5.3) Vancomycin calibration curve

The vancomycin standard solution at the concentration of 10, 20, 30, 40, 50, 60, 80, 100, 150 and 200 ppm were prepared in aqueous solution and in SBF solution. The absorbance of the drugs was measured.

5.4) Drug loading

Approximately 1 g of the 3DOM HAp and the 3DOM FeHAp were place into a PE centrifuge tube containing vancomycin drug solution. The mixture was stirred at room temperature for 24 hours. After that, the 3DOM HAp and the 3DOM FeHAp were separated from the solution by filtration using sieve glass. The drug concentration in

filtrate was determined by measuring absorbance. The 3DOM HAp and the 3DOM FeHAp were washed with deionized water and then dried at 110°C for 1 hour. In most case, the dilution of filtrate was carried out in order to keep the sample concentration within a range of the calibration curve.

5.5) Drug releasing

After drug loading process, the 3DOM HAp and the 3DOM FeHAp were immersed in 6 ml of SBF solution in a PE centrifuge tube at 37 °C. The mixture was stirred and centrifuged. The 5 ml of centrifugate was collected for an UV absorption study and then the 5 ml of fresh SBF were added into the PE centrifuge tube. The process was repeatd for 24 hours. The drug release percentage was calculated using Eq. 3.

$$\% \text{ drug release} = \frac{\text{total amount of release drug (µg/g)}}{\text{loading drug per gram of HAp (µg/g)}} \times 100 \qquad \text{(eq 3)}$$

Results and Discussions

1) Characterization of monodispersed PMMA microsphere

The SEM images of the synthesized PMMA spheres exhibited monodispered particles with approximate diameter of 340±10 nm. The SEM micrograph also revealed that the PMMA arrays were well ordered with cubic-closest packed arrangement as showed in Fig. 5.

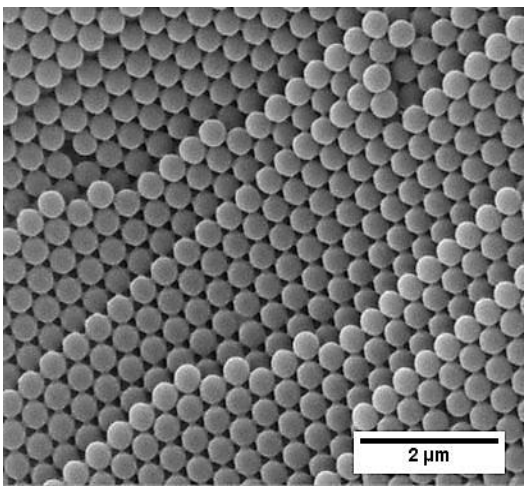

Figure 5 The SEM micrograph of PMMA colloidal spheres.

2. Characterization of 3DOM HAp and 3DOM Fe HAp

2.1 Morphology analysis of the 3DOM HAp and 3DOM FeHAp

After calcinations, the produced 3DOM HAp was white, in contrary to the yellow brown 3DOM FeHAp (Fig. 6). Both 3DOM materials, however, exhibited an iridescent phenomenon which could be implied that the three dimensionally ordered structures were maintained after calcination. These would be further confirmed by SEM analysis.

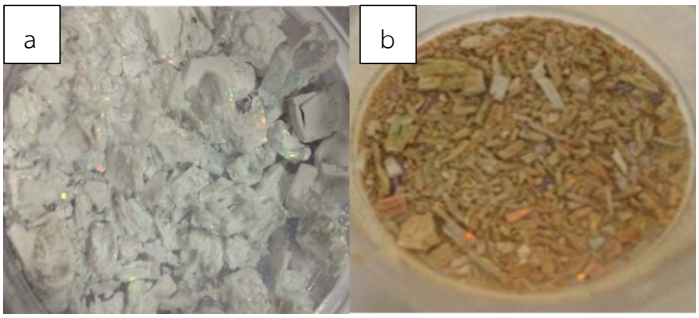

Figure 6 Visual appearance of the synthesized (a) 3DOM HAp and (b) 3DOM FeHAp.

The surface morphology of the calcined 3DOM HAp, 3DOM FeHAp 7%mol, 3DOM FeHAp 14%mol, 3DOM FeHAp 21%mol, and 3DOM FeHAp 28%mol are shown in Fig. 7. It could be seen that all materials were highly ordered macroporosity with interconnected wall. The average open window diameter is approximately 260±10 nm. The decrease in the diameter of the open window could be caused by shrinkage of the HAp for all samples framework during the calcination of process.

The elemental analysis using EDX of the 3DOM HAp and the 3DOM FeHAp were carried out. The results showed that Ca, P, and O were observed in both 3DOM materials while the additional Fe was only observed in the 3DOM FeHAp.

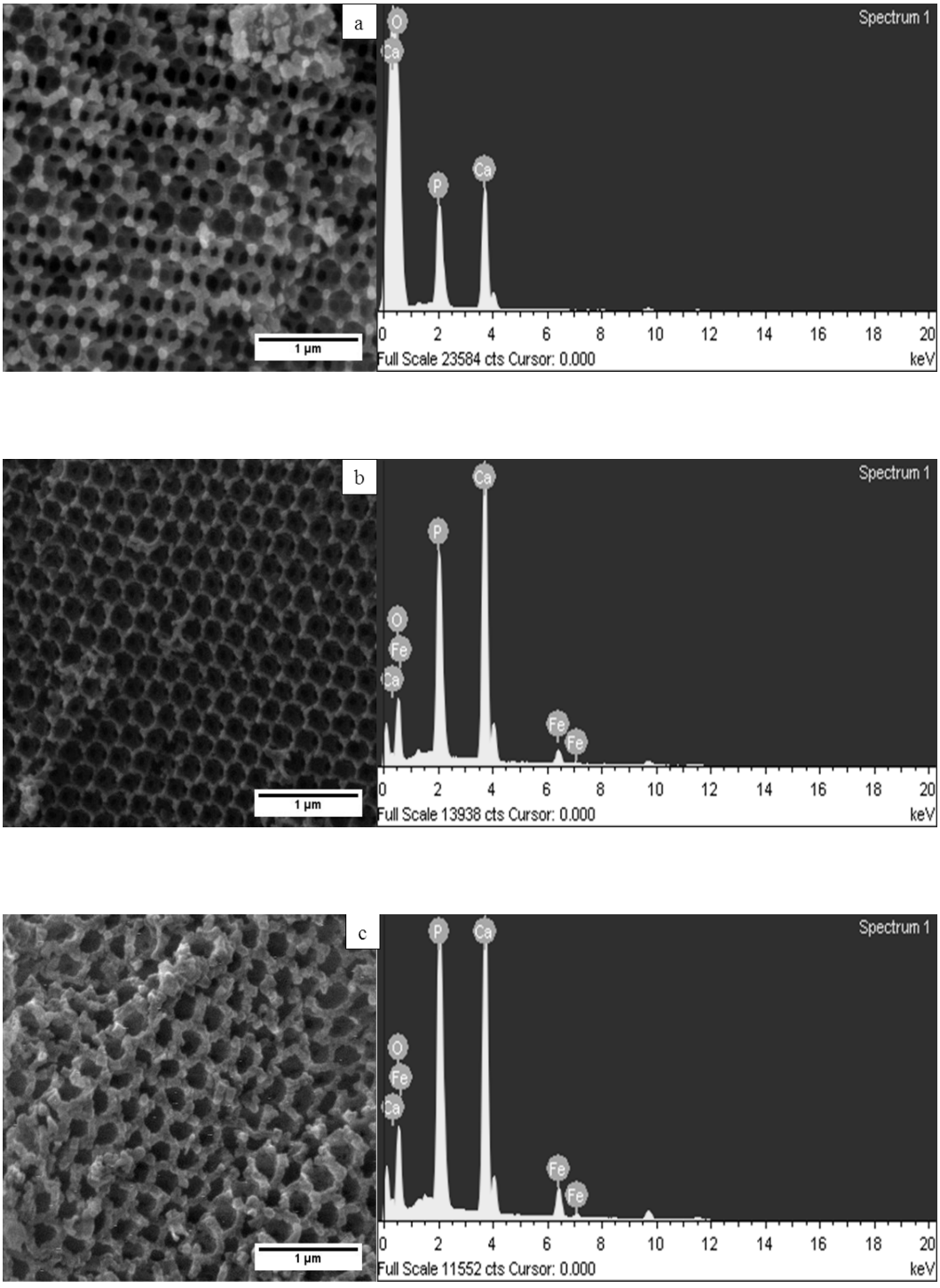

Figure 7 The SEM micrograph of a) 3DOM HAp b) 3DOM FeHAp 7% mol,

c) 3DOM FeHAp 14% mol, d) 3DOM FeHAp 21% mol, and e) FeHAp 28% mol

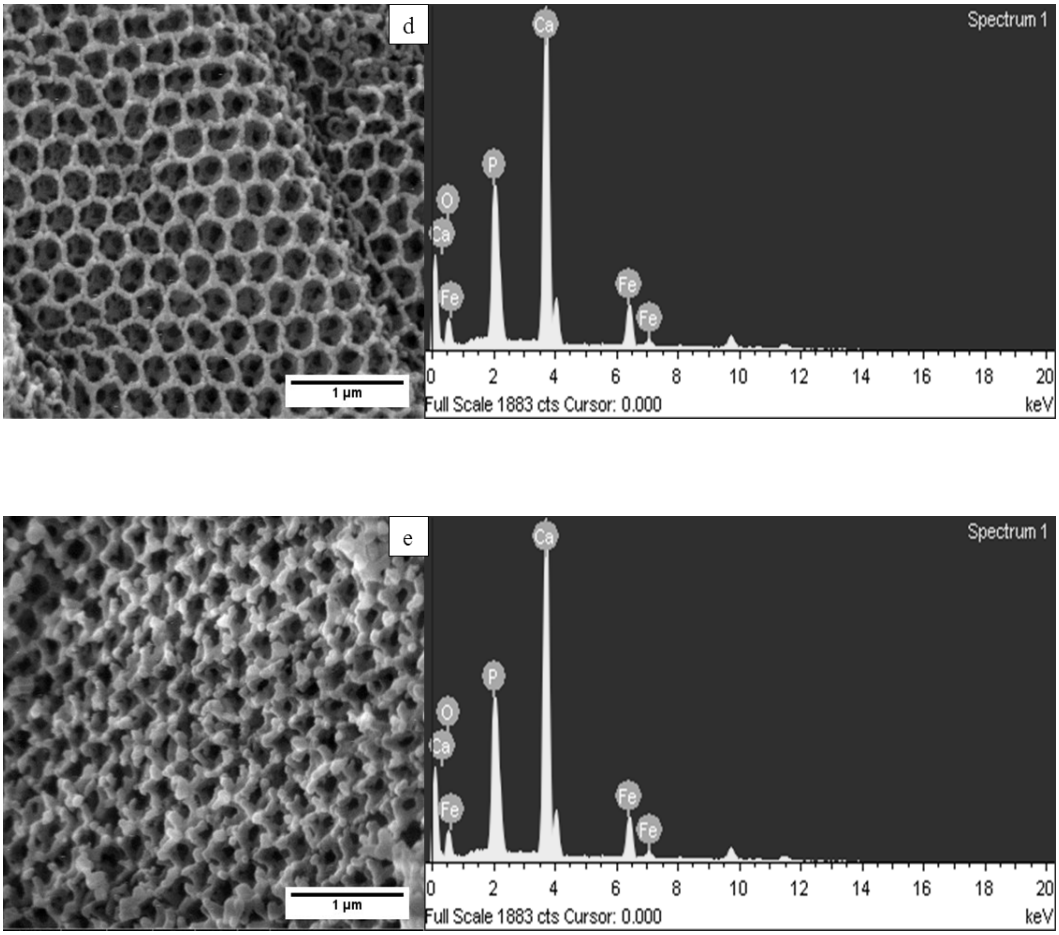

Figure 7 (Continued)

2.2 FTIR analysis

The Fourier transform infrared technique (FTIR) was employed as a preliminary technique in order to examine a hydroxyl and a phosphate group of the HAp. The FTIR spectra of the 3DOM HAp and the 3DOM FeHAp are shown in Fig. 8. The characteristic IR absorption peak of the 3DOM HAp and the 3DOM FeHAp 7% mol-28% mol are shown Table 3. The vibrational patterns of all 3DOM HAp displayed characteristic vibrations of OH^- group at 603 cm^{-1} and 3565 cm^{-1}, PO_4^{3-} apatite group at 961 cm^{-1} ($\mathbf{U}_1$), 474 cm^{-1} ($\mathbf{U}_2$),

1040 cm^{-1} ($\mathbf{U}_3$), and at 603 and 570 cm^{-1} ($\mathbf{U}_4$). The absorption peaks at 870 and 1456 cm^{-1} were corresponded to CO_3^{2-} group of $CaCO_3$ [50]. The results indicated that the synthesized materials are in apatite group. Further study by XRD analysis should be employed to confirm that the 3DOM HAp were successfully synthesized by sol-gel technique.

Compared to the FTIR spectrum of the conventional HAp, the FTIR spectra of the 3DOM HAp and the 3DOM FeHAp 7-28% mol showed no significant differences in absorption patterns, indicating that all materials maintained a similar chemical structure. (Tseng *et al*., 2014). The FTIR spectra of all 3DOM HAp were well agreed with previous study [51]. In addition, carbon dioxide *(CO_2)* absorption bands were noticeable within all spectra.

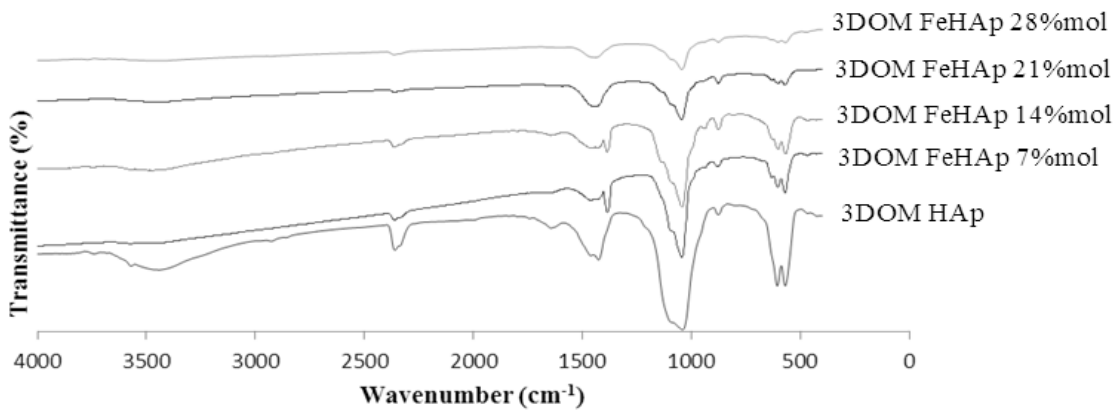

Figure 8 The FTIR spectra of the 3DOM HAp and the 3DOM FeHAp 7% - 28% mol.

Table 3 Characteristic absorption peaks of the synthesized 3DOM HAp and 3DOM FeHAp from sol-gel process.

	PO_4^{3-} vibration				CO_3^{2-} vibration		O-H vibration	
3DOM	Bending	Stretching	Stretching	Stretching	Bending	Stretching	Vibration	Stretching
	υ_2	υ_4	υ_1	υ_3	υ_1	υ_2	δ_1	υ_2
HAp	474	570, 603	961	1040	870	1421, 1456	628	3565
FeHAp 7% mol	469	571, 603	939	1041	877	1384, 1456	630	3571
FeHAp 14% mol	474	568, 603	962	1041	875	1385, 1460	629	3440
FeHAp 21% mol	463	570, 603	960	1044	876	1443, 1593	629	3464
FeHAp 28% mol	473	568, 603	960	1044	876	1441, 1593	629	3467

2.3 XRD phase analysis

The XRD pattern of the 3DOM HAp and the 3DOM FeHAp 7% mol at various aging times are shown in Figure 9 and 10. All XRD spectra are in good agreement with the standard HAp diffraction pattern from the Joint Committee on Powder Diffraction Standards JCPDS card 01-089-6437 of HAp. The phase composition of the produced 3DOM HAp and 3DOM FeHAp 7% mol are shown in Table 4. The lower aging time resulted in lower HAp phase composition and also lower crystallinity as broaden peaks were observed [52]. When the aging time was increased, the phase composition of HAp phase became higher with maxima of 77.01% after 10 hours aging time. The XRD spectrum of the 3DOM FeHAp 7%mol exhibited no other Fe-containing composition which may be implied that all Fe were incorporated into HAp structure giving 78.41% of the HAp phase at 8 hours aging time.

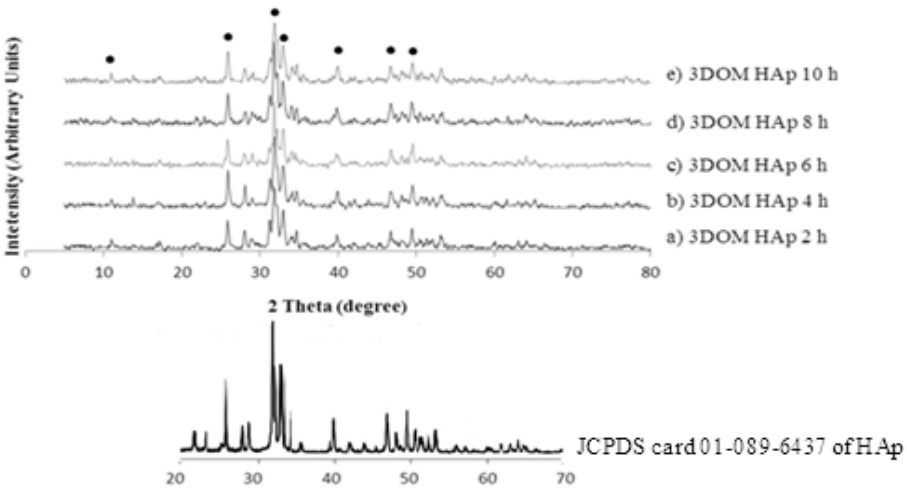

Figure 9 XRD patterns of the 3DOM HAp at various aging times. (● = HAp phase)

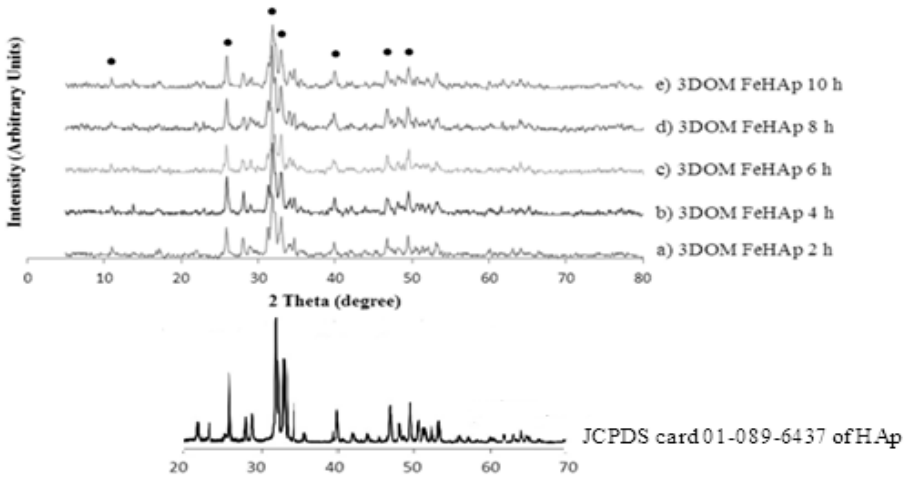

Figure 10 XRD patterns of the 3DOM FeHAp 7%mol at various aging times. (● = HAp phase)

Table 4 The effect of aging time on the phase composition of the synthesized 3DOM HAp and 3DOM FeHAp 7%mol.

Sample 3DOM	Stirring time (h)	Aging time (h)	Phase composition (%) HAp	$Ca_3(PO_4)_2$	$CaCO_3$	CaO
HAp2	4	2	69.55	17.21	11.86	1.38
HAp4	4	4	72.35	15.14	11.29	1.23
HAp6	4	6	72.62	16.82	9.44	1.12
HAp8	4	8	74.85	16.17	7.74	1.24
HAp10	4	10	77.01	16.01	6.96	0.02
FeHAp2	4	2	68.03	25.69	5.39	0.90
FeHAp4	4	4	72.80	24.71	1.96	0.53
FeHAp6	4	6	75.22	13.99	9.74	1.08
FeHAp8	4	8	78.41	14.60	6.45	0.54

FeHAp10	4	10	71.09	25.65	2.51	0.75

ICP-OES examination was also conducted to further confirm the element content in the 3DOM HAp and the 3DOM FeHAp 7%mol (Table 5). The Ca/P mole ratio for the 3DOM HAp is 1.64 which is close to the typical 1.67 Ca/P ratio for HAp mole ratio. For the 3DOM FeHAp, the Ca+Fe/P molar ratio is higher than 1.67 due to addition of Fe content. From ICP-OES results, the synthesized 3DOM HAp is Ca-deficient HAp from its low Ca/P mole ratio (Li *et al*., 2012). On the other hand, the high Ca+Fe/P ratio in the 3DOM FeHAp indicated that other trace compound containing Ca ions may be found in the 3DOM FeHAp as minor phase.

Table 5 Composition of 3DOM HAp and 3DOM FeHAp 7% mol determined by ICP-OES.

Element(Concentration)	Sample	
	3DOM HAp	3DOM FeHAp 7%mol
Ca (wt%)	36.29	34.38
P (wt%)	17.09	16.02
Fe (wt%)	-	3.10
Ca/P (mole ratio)	1.64	1.77

All 3DOM FeHAp (7-28 % mol) showed characteristic of the HAp peaks without significant alternations or peak shift, regardless of Fe concentrations. This suggested that the iron substituted HAp process did not greatly modify the structure of the HAp. On the other hand, minor phase of Fe_3O_4 was observed in the 3DOM FeHAp 14%-28%mol as a result of increasing concentration of iron. It may be seen that all 3DOM FeHAp showed a

decreasing in the HAp phase when the iron concentration was increased. The percentages of phase compositions were listed in Table 6.

Table 6 Phase composition of the 3DOM HAp and the 3DOM FeHAp from XRD analysis.

	Phase composition *(%)*				
Sample 3DOM	HAp	$Ca_3(PO_4)_2$	$CaCO_3$	CaO	Fe_3O_4
HAp	77.01	16.01	6.96	0.02	-
FeHAp 7% mol	78.41	14.60	6.45	0.54	-
FeHAp 14% mol	62.19	20.89	15.55	0.66	0.71
FeHAp 21% mol	61.38	25.71	10.19	1.43	1.30
FeHAp 28% mol	56.70	36.26	5.72	0.79	0.54

The crystallite size of all 3DOM materials can be calculated using Scherrer's equation (Eq 4), as presented in Table 7.

$$d = \frac{0.89\lambda}{\beta\cos\theta} * \frac{180}{\pi} \qquad \text{(eq 4)}$$

: d = mean size of the ordered (crystalline) domains, which may be smaller or equal to the grain size (nm)

λ = the wavelength of x-ray beam (1.5406 nm for Cu Kα radiation)

β, FWHM = the full width at half maximum for the diffraction peak under consideration (rad)

θ = the diffraction angle (°).

Table 7 The calculated crystallite sizes of the 3DOM HAp and the 3DOM FeHAp.

Product	FWHM	Diffraction angle (2θ)	Crystallite size (nm)
3DOM HAp	0.363	31.898	22.2
3DOM FeHAp 7%mol	0.328	31.791	24.6
3DOM FeHAp 14%mol	0.378	31.840	21.4
3DOM FeHAp 21%mol	0.375	31.861	21.6
3DOM FeHAp 28%mol	0.227	31.812	35.6

It can be seen that the 3DOM HAp and the 3DOM FeHAp 7-21%mol remained crystalline with similar FWHM value at diffraction angle approximately 31.8 (2θ). As a result, calculated crystallite size were comparable.

2.4 Surface area analysis

The specific surface area of HAp was calculated based on Brunauer Emmett and Teller *(*BET*)* equation (Brunauer *et al.,* 1938). The specific surface area of the 3DOM HAp, 3DOM FeHAp 7% mol, 3DOM FeHAp 14% mol, 3DOM FeHAp 21% mol, and 3DOM FeHAp 28% mol were 62.1, 86.1, 61.3, 62.8 and 28.4 m^2/g, respectively. The pore volume was determined using the Barrelt-Joyner-Halenda (BJH) method [53, 54] and listed in Table 8. It was found that the 3DOM FeHAp 28%mol have the lowest surface area compared to the other samples. This was probably due to the deformation of the pore morphology of the 3DOM structure.

Table 6 Physiochemical properties of the 3DOM HAp and the 3DOM FeHAp materials.

Sample	Surface Area (m^2/g)	Pore volume cm^3/g	Pore Size (nm)
3DOM HAp	62.1	0.208	3.4
3DOM FeHAp 7% mol	86.1	0.249	3.0
3DOM FeHAp 14% mol	61.3	0.250	9.5
3DOM FeHAp 21% mol	62.8	0.341	3.0
3DOM FeHAp 28% mol	28.4	0.202	3.8

2.5 Magnetic property

The magnetization of the 3DOM HAp and the 3DOM FeHAp with 7%-28% mol of Fe were shown in Fig. 11. It was found that the magnetic property of the 3DOM HAp and the 7% mol 3DOM FeHAp was gradually increased with an increasing external magnetic field. This indicated that both 3DOM materials are paramagnetic with the maximum magnetization of 0.068 and 0.222 emu g^{-1} for the 3DOM HAp and the 3DOM FeHAp 7%mol, respectively. On the other hand, the 3DOM FeHAp with 14-28% mol are superparamagnetic with narrow hysteresis loop [55]. The saturation magnetization *(M_s)* of the 14-28% mol 3DOM FeHAp are 0.600, 0.788 and 1.556 emu g^{-1}, respectively *(*Figure 13*)*. The hysteresis loop of all 3DOM biomaterials are symmetrical, indicating on uniform distribution of Fe in all 3DOM FeHAp [10]**.**

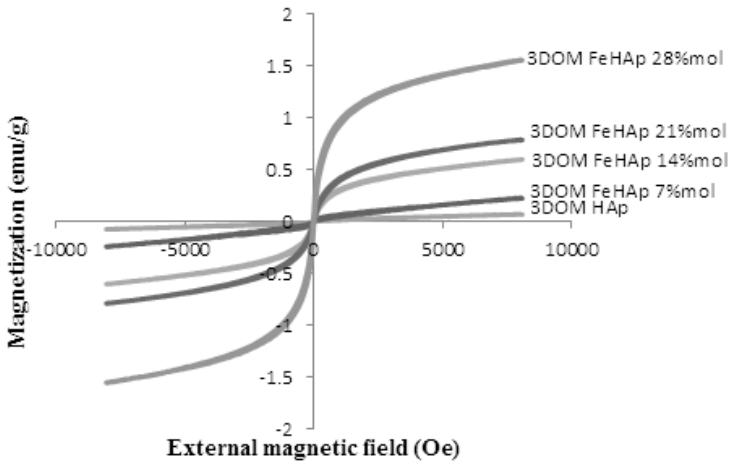

Figure 11 Magnetization curves of 3DOM HAp and 3DOM FeHAp.

3. Cytotoxicity study of the 3DOM HAp and the 3DOM FeHAp

3.1 Cell viability or Cytotoxicity test

The viability of osteoblast cells by MTS method was shown in Figure 12. Briefly, the 3DOM HAp and the 3DOM FeHAp at various concentration (*2000* μg/ml; *1000* μg/ml; *500* μg/ml; *250* μg/ml) were immersed in the medium for 24 hours. The medium was further used as a culture media for the osteoblast cells. The ANOVA statistic program was employed to analyze the suitability of the data. It was found that the deviation of data points were $p < 0.05$. The results demonstrated that the 3DOM HAp and all 3DOM FeHAp did not cause significantly reduction of cell viability. However, the cell viability of the 3DOM FeHAp 28% mol with concentration of 2000 μg/ml may be slightly low. It may be due to a possible release of transition ions to the media resulting in higher toxicity to the cells.

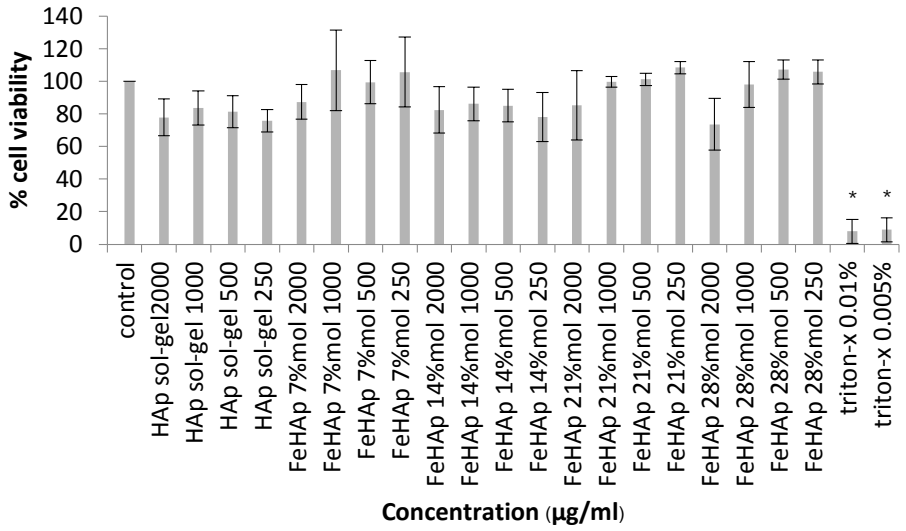

Figure 12 The percentage of cell viability of the 3DOM HAp and the 3DOM FeHAp 7%-28%mol *(*ANOVA (Dunnett t (2-sided)) significant at $p < 0.05$*)*.

3.2 Cell attachment

The biocompatibility of the 3DOM HAp and the 3DOM FeHAp were confirmed by fluorescence staining and SEM. After 24 hours of cell cultivation, the osteoblast cells were plated onto the 3DOM HAp and 3DOM FeHAp substrates. In Figure 13 and 14, it can be seen that the nuclei (blue) and cytoskeleton (tubulin green) of the cells were detected on the 3DOM HAp and on the 3DOM FeHAp, respectively. The fluorescence images showed that the cells attached on the 3DOM materials with a typical osteoblast cell conformation.

Figure 15 shows the SEM image of the osteoblast cells on the surface of the 3DOM HAp and the 3DOM FeHAp 7%mol after 24 hours of incubation. Backscattered electron images showed the osteoblast cell in the darker phase *(*lower atomic number*)* and the 3DOM FeHAp 7%mol *(*higher atomic number*)* in the lighter contrast. The SEM images

showed that osteoblast attached only on the 3DOM surface due to the 3DOM pore size which were significantly smaller than the cell *(*10-15 μm*)*.

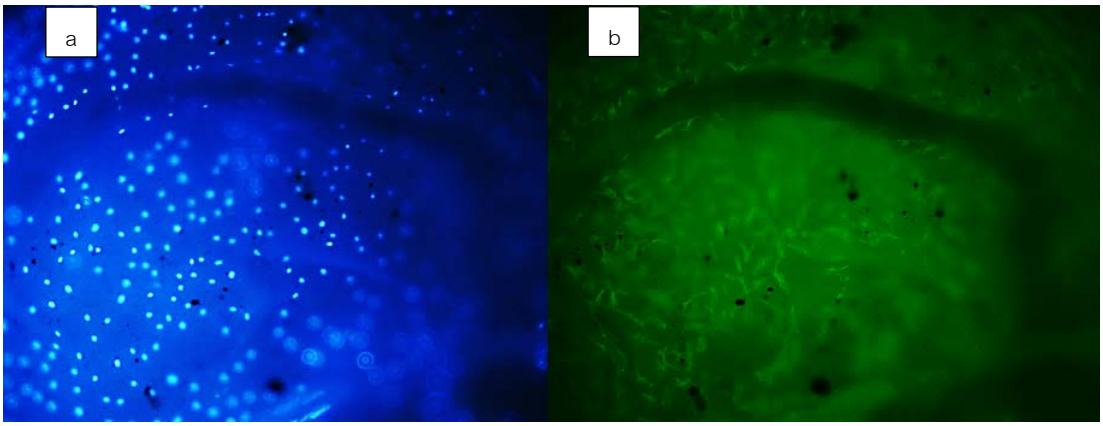

Figure 13 *(a)* Nuclei *(*blue*)* and *(b)*cytoskeleton *(*tubulin green*)* staining of osteoblasts on 3DOM HAp.

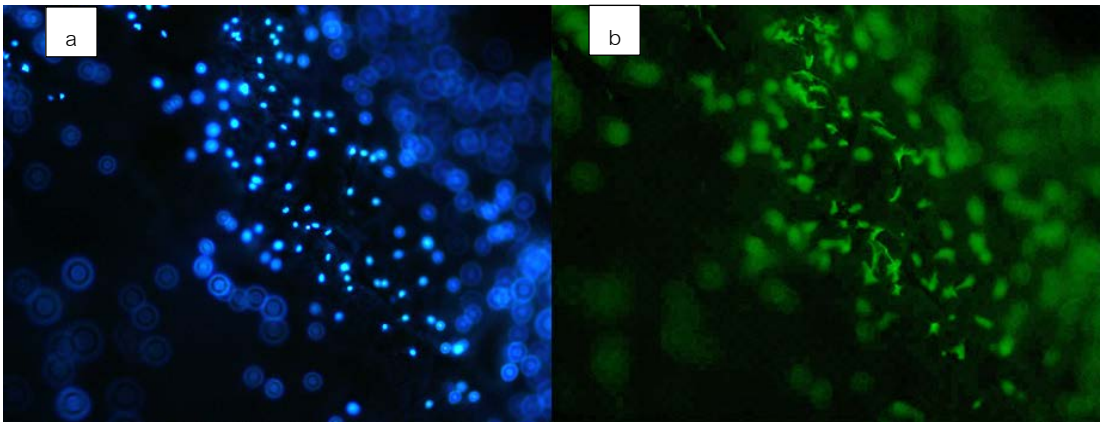

Figure 14 (a) Nuclei (blue) and (b) cytoskeleton (tubulin green) staining of osteoblasts on 3DOM FeHAp.

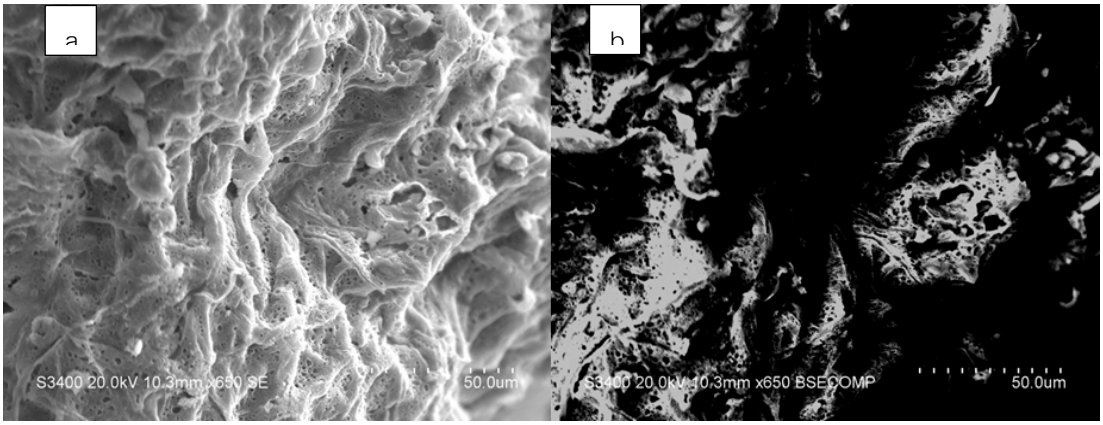

Figure 15 SEM image of cell morphology on the surface of 3DOM FeHAp after incubation with osteoblasts.

4. Antibiotic drug delivery using the 3DOM HAp and the 3DOM FeHAp as a drug carrier

The application of the 3DOM the HAp and the 3DOM FeHAp 7%mol as drug delivery carrier was examined using antibiotic drug, vancomycin. Among the synthesized 3DOM FeHAp, the 3DOM FeHAp 7%mol was chosen here because of its uniformly pore size, interconnected pores, and high surface area. The calibration curve of vancomycin in both water and SBF was studied. The drug loading efficiency and drug release profile of the 3DOM materials were also investigated.

4.1 Calibration curve of vancomycin in water and in SBF

Various concentrations of vancomycin (10-200 ppm) were prepared in aqueous solution and in SBF, and their absorbance was measured at 281 nm. The absorbance data (Table 9 and 10) were plotted against the concentration of vancomycin in aqueous solution and in SBF, to obtain the calibration curves (Fig. 16 and 17).

Table 9 The absorbance of vancomycin in aqueous solution, measured at 281 nm.

Concentration	absorbance of vancomycin in aqueous solution			
(ppm)	I	II	average	SD
10	0.047	0.047	0.047	0.000
20	0.098	0.102	0.100	0.003
30	0.144	0.142	0.143	0.001
40	0.183	0.183	0.183	0.000
50	0.235	0.234	0.235	0.001
60	0.273	0.266	0.270	0.005
80	0.357	0.361	0.359	0.003
100	0.449	0.448	0.449	0.001
150	0.642	0.643	0.643	0.001
200	0.881	0.882	0.882	0.001

Table 10 The absorbance of vancomycin in SBF, measured at 281 nm.

Concentration	absorbance of vancomycin in SBF			
(ppm)	I	II	average	SD
10	0.036	0.037	0.037	0.001
20	0.079	0.080	0.080	0.001
30	0.166	0.167	0.167	0.000
40	0.171	0.171	0.171	0.001
50	0.208	0.208	0.208	0.000
60	0.258	0.258	0.258	0.000
80	0.342	0.342	0.342	0.000
100	0.423	0.422	0.423	0.001
150	0.642	0.641	0.642	0.001
200	0.847	0.848	0.848	0.001

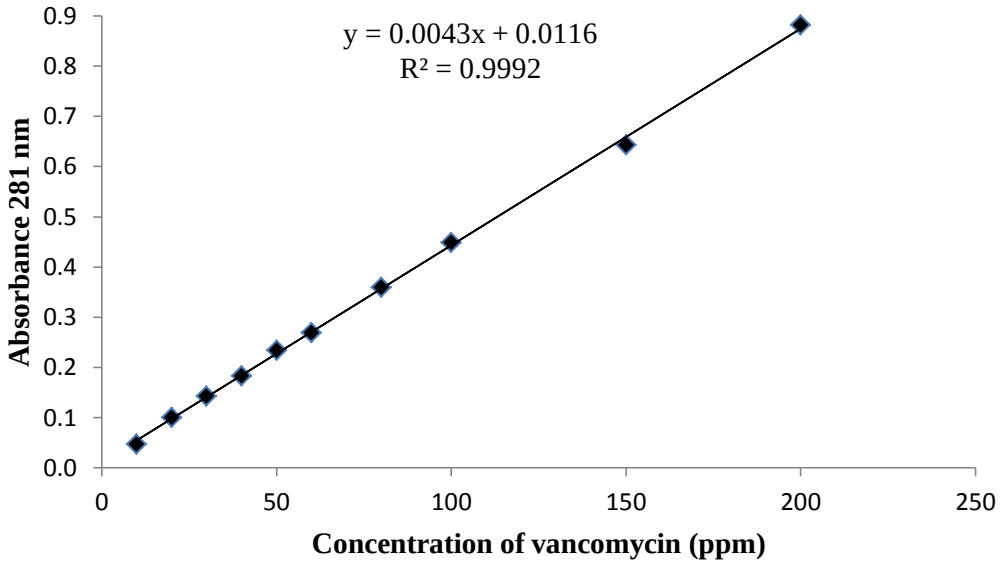

Figure 16 The calibration curve of vancomycin in aqueous solution.

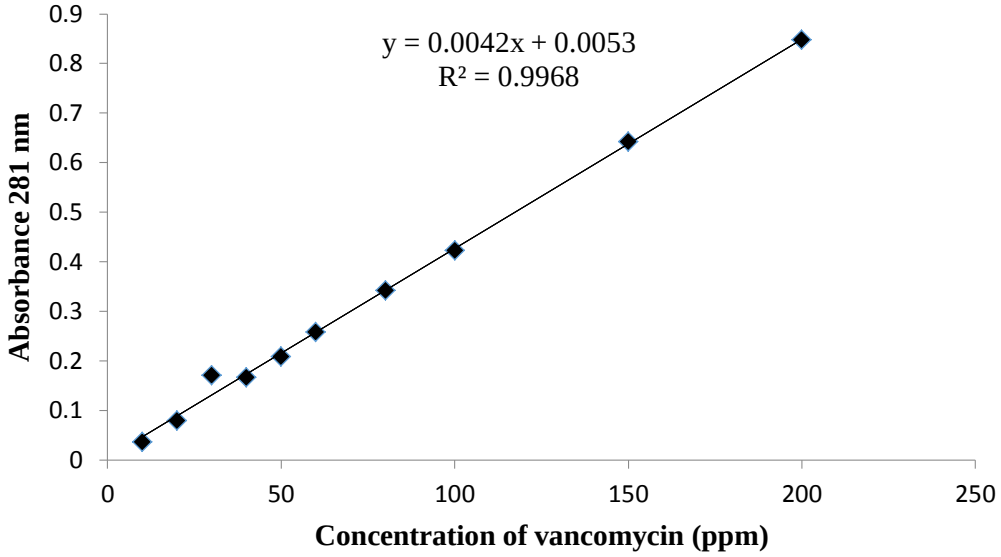

Figure 17 The calibration curve of vancomycin in SBF.

4.2 Drug loading

To examine the drug loading efficiency of the 3DOM HAp and the 3DOM FeHAp, the synthesized materials were immersed in vancomycin solution (2000 ppm, 5 ml) for 24 hours. The HAp derived from natural material was also studied to compare the drug loading ability with the 3DOM materials. After 24 hours of immersion in the drug solution, the mixture was filtered, and the filtrate was measured at 281 nm by UV-VIS spectrometer. The drug loading per one gram of the 3DOM HAp, the 3DOM FeHAp 7%mol, and HAp from natural material were 1338.87, 1318.46 and 327.87 μg/g, respectively *(*Table 11*)*. It could be seen that the highest amount of vancomycin loading in HAp was found in the case of 3DOM HAp, both pure HAp and iron substituted HAp. This could be due to the three dimensionally ordered structure and interconnected pores of the synthesized 3DOM HAp that may facilitate drug-loading process.

4.3 Drug release

In this study, drug release profiles of the HAp materials were investigated by immersing 0.2 g of either the drug loaded 3DOM materials or the HAp from natural material in 6 ml of SBF solution at 37 °C. A 5 ml of the SBF supernatant was collected at 0, 0.5, 1, 2, 6, 10, 14, 18, 22, and 24 hours and replaced with 5 ml of fresh SBF. The absorbance of the collected supernatant was measured at 281 nm. Calculation of percentage of drug released from HAp in SBF solution is exhibited in Table 12.

Table 11 Calculation of drug loading in HAp in aqueous solution.

Sample	Weight of HAp (g)	Absorbance	Concentration (ppm)	Dilution factor	Drug concentration in 5 ml solution (ppm)	loading drug (ppm)	loading drug per gram of HAp (ppm/g)	%drug loading
Before load		0.864	197.30	10	1973.00			
After load								
3DOM HAp	1.0005	0.284	63.30	10	633.41	1339.53	1338.87	67.8
Before load		0.865	198.50	10	1984.65			
After load								
3DOMFeHAp7%mol	1.0054	0.295	65.90	10	656.07	1325.58	1318.46	66.7
Before		0.875	200.79	10	2000.91			
After load								
*HAp from natural materials	1.0001	0.734	168.00	10	1680.00	327.91	327.87	16.3

* HAp from natural materials by Phumthiean, 2013 [14].

Table 12 Calculation of percentage of drug released from HAp in SBF solution.

Sample	Weight of loaded HAp (g)			Total amount of release (μg)	Loading drug per gram of HAp (μg/g)	% drug release
	1	2	average			
3DOM HAp	0.2002	0.2020	0.2011	965.96	1338.87	72.1
3DOM FeHAp 7%mol	0.2062	0.2045	0.2054	1062.86	1318.46	80.6
*HAp from natural materials	0.2000	0.2000	0.2000	104.76	327.87	33.1

* HAp from natural materials by Phumthiean, 2013 [14].

The cumulative profile of vancomycin release from the 3DOM HAp, 3DOM FeHAp 7%mol, and HAp from natural materials are given in Figure 18. It can be seen that all samples showed a biphasic drug release profile (an rapid initial release followed by a slow release). Approximately 72.1% and 80.6% of vancomycin were released from the 3DOM HAp and the 3DOM FeHAp over 24 hours, while only 33.1% of the drug release was found in the case of HAp from natural material. The lower vancomycin released in the HAp from natural material is to its lower surface area. The drug release experiment of the HAp from natural material was carried out before that of the 3DOM materials, and the experiment was stopped after 4 hours since no vancomycin was detected in the SBF supernatant after that period of time.

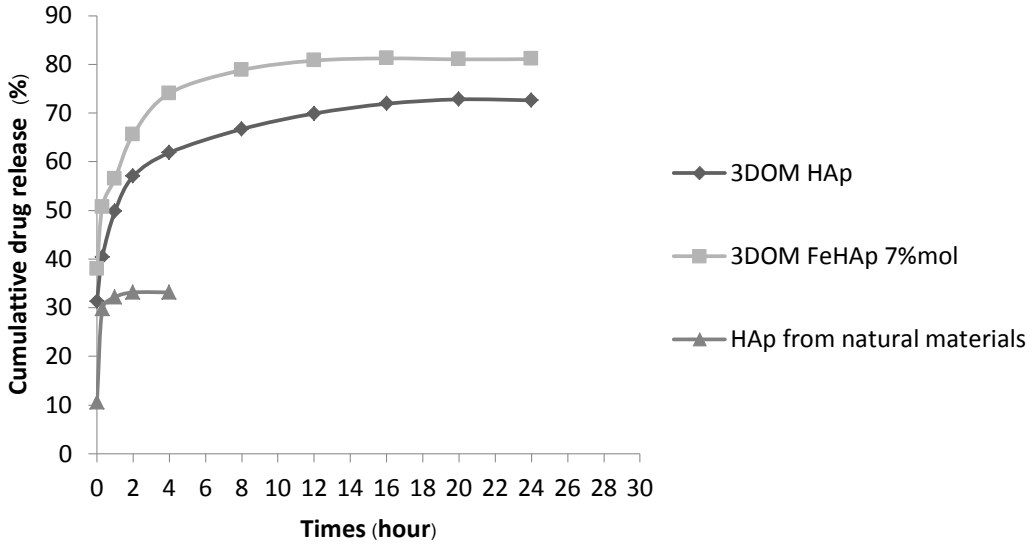

Figure 36 The percentage of cumulative vancomycin release in SBF solution as function of time.

From the study, the amount of loaded vancomycin into the 3DOM HAp and the 3DOM FeHAp are significantly higher than that of the HAp from natural material showed in (Table 13). The lower vancomycin concentration in the HAp from natural material is likely due to its lower surface area. For the 3DOM materials, the open network with interconnected pores greatly benefits the drug loading into the HAp structure reaching the maxima of 67.8%.

In addition, the loaded vancomycin in the 3DOM materials were released upto 72.1% in the 3DOM HAp and 80.6% in the 3DOM FeHAp. It can be concluded that the hierarchical structure with interconnected pore is a great advantage for the 3DOM HAp and the 3DOM FeHAp to be used as a drug carrier for drug delivery application.

Table 13 The percentage of drug loading and drug release from various HAp sample.

Sample	Surface Area (m^2/g)	Wt % drug loading	Wt % drug releasing
3DOM HAP	62.1	67.8	72.1
3DOM FeHAp 7%mol	86.1	66.7	80.6
HAp from natural materials	20.9	16.3	33.1

* HAp from natural material

CONCLUSION

Three dimensionally ordered macroporous hydroxyapatite (3DOM HAp) and iron substituted 3DOM HAp was successfully synthesized by sol-gel method using PMMA colloidal crystal arrays. The PMMA microspheres with approximate diameter of 360±19.25 nm were prepared via emulsifier free emulsion polymerization. The 3DOM HAp and all 3DOM FeHAp using PMMA with diameter of 360 nm as templates exhibited interconnected pore with approximately diameter pore size of 260±10 nm. The FTIR spectra of the 3DOM HAp and all 3DOM FeHAp displayed characteristic vibrations of the phosphate (PO_4^{3-}), carbonate (CO_4^{3-}), and hydroxyl (-OH) groups. The surface area of 3DOM HAp 3DOM FeHAp 7%mol, 3DOM FeHAp 14%mol, 3DOM FeHAp 21%mol, and 3DOM FeHAp 28%mol using BET showed surface area of were 62.1, 86.1, 61.3, 62.8 and 28.4 m^2/g, respectively.

The characterization of the 3DOM HAp and 3DOM FeHAp structure was confirmed using XRD patterns. Preliminary studies of suitable aging time for the 3DOM HAp is 10 hours resulting in 77.01% of HAp. The XRD spectrum of the 3DOM FeHAp 7%mol exhibited no other Fe-containing phase giving 78.41% of HAp phase at aging time 8 hours. The XRD pattern of 3DOM HAp, 3DOM FeHAp 7%mol, 3DOM FeHAp 14%mol, 3DOM FeHAp 21%mol, and the 3DOM FeHAp 28%mol gave highest percentage of HAp phase at 77.01%, 78.41%, 62.19%, 61.38%, and 56.70%, respectively.

The study of the magnetization properties of 3DOM HAp revealed that 7%mol Fe doped HAp was paramagnetic. The 3DOM FeHAp 14-28%mol were superparamagnetic. The 3DOM FeHAp 28%mol gives highest magnetization at 1.556 emu g^{-1}. Potentially, the synthesized 3DOM FeHAp may be further modified to produce a hierarchical ferromagnetic HAp material.

Cytotoxicity study suggested that all samples were non-cytotoxic to osteoblasts. However, the 3DOM HAp and 3DOM FeHAp 7%mol do not facilitate the osteoblast differention. Osteoblast cells can be attachment and grown on the 3DOM structure and interconnect pore.

The study of drug carrier property of the 3DOM HAp and the 3DOM FeHAp 7%mol using vancomycin was investigated. It is found that high surface area and hierarchical structure of the 3DOM HAp and the 3DOM FeHAp greatly enhance the efficiency of drug loading into the synthesized hydroxyapatite. In addition, the amount of drug released from the 3DOM HAp and the 3DOM FeHAp 7%mol were between 72.1% - 80.6% of total loading drug which 33.1% was observed in the HAp from natural product. Therefore, the 3DOM HAp and the 3DOM FeHAp are a promising biomaterial for drug delivery applications.

References

1. Gibson, I.R., S.M. Best, and W. Bonfield, *Effect of Silicon Substitution on the Sintering and Microstructure of Hydroxyapatite.* Journal of the American Ceramic Society, 2002. **85**(11): p. 2771-2777.
2. With, G., et al., *Preparation, microstructure and mechanical properties of dense polycrystalline hydroxy apatite.* Journal of Materials Science, 1981. **16**(6): p. 1592-1598.
3. Kim, S.R., et al., *Synthesis of Si, Mg substituted hydroxyapatites and their sintering behaviors.* Biomaterials, 2003. **24**(8): p. 1389-1398.
4. Webster, T.J., et al., *Osteoblast response to hydroxyapatite doped with divalent and trivalent cations.* Biomaterials, 2004. **25**(11): p. 2111-2121.

5. Xu, J.L. and K.A. Khor, *Chemical analysis of silica doped hydroxyapatite biomaterials consolidated by a spark plasma sintering method.* Journal of Inorganic Biochemistry, 2007. **101**(2): p. 187-195.
6. Anee, T.K., et al., *Influence of iron and temperature on the crystallization of calcium phosphates at the physiological pH.* Materials Letters, 2004. **58**(3–4): p. 478-482.
7. Mornet, S., et al., *Magnetic nanoparticle design for medical diagnosis and therapy.* Journal of Materials Chemistry, 2004. **14**(14): p. 2161-2175.
8. Vallet-Regi, M., *Ceramics for medical applications.* Journal of the Chemical Society, Dalton Transactions, 2001(2): p. 97-108.
9. Panseri, S., et al., *Intrinsically superparamagnetic Fe-hydroxyapatite nanoparticles positively influence osteoblast-like cell behaviour.* Journal of Nanobiotechnology, 2012. **10**(1): p. 32.
10. Sarath Chandra, V., et al., *Blood Compatibility of Iron-Doped Nanosize Hydroxyapatite and Its Drug Release.* ACS Applied Materials & Interfaces, 2012. **4**(3): p. 1200-1210.
11. Li, J., et al., *Macroporous ordered titanium dioxide (TiO2) inverse opal as a new label-free immunosensor.* Analytica Chimica Acta, 2008. **625**(1): p. 63-69.
12. Li, S., et al., *Preparation and characterization of three-dimensional ordered macroporous ZrO2 by two-step templating process.* Journal of Porous Materials, 2009. **16**(5): p. 553-556.
13. Xia, Y., et al., Adv. Mater., 2000. **12**: p. 693.
14. Phumthiean, N., *Development and Charaterization of Three-Dimensionally Ordered Macroporous Hydroxyapatite (3DOM HAp) by Sol-Gel Technique and Its Application as Vancomycin Drug Carrier*, in *Department of Chemistry*. 2013, Kasetsart University. p. 132.
15. Tampieri, A., et al., *Intrinsic magnetism and hyperthermia in bioactive Fe-doped hydroxyapatite.* Acta Biomaterialia, 2012. **8**(2): p. 843-851.
16. Prijic, S., et al., *Increased cellular uptake of biocompatible superparamagnetic iron oxide nanoparticles into malignant cells by an external magnetic field.* J Membr Biol, 2010. **236**: p. 167 - 179.
17. Kasten, A., et al., *Mechanical integrin stress and magnetic forces induce biological responses in mesenchymal stem cells which depend on environmental factors.* J Cell Biochem, 2010. **111**: p. 1586 - 1597.

18. Ajeesh, M., et al., *Nano iron oxide–hydroxyapatite composite ceramics with enhanced radiopacity.* Journal of Materials Science: Materials in Medicine, 2010. **21**(5): p. 1427-1434.
19. Yan, L., N. Chai Teck, and O. Chui Ping, *Iron(III) and manganese(II) substituted hydroxyapatite nanoparticles: Characterization and cytotoxicity analysis.* Journal of Physics: Conference Series, 2009. **187**(1): p. 012024.
20. Filho, F.P., et al., *Structural and mechanical study of the sintering effect in hydroxyapatite doped with iron oxide.* Physica B: Condensed Matter, 2008. **403**(19–20): p. 3826-3829.
21. Parelman, M., et al., *Iron restriction negatively affects bone in female rats and mineralization of hFOB osteoblast cells.* Exp Biol Med (Maywood), 2006. **231**: p. 378 - 386.
22. Melde, B.J. and A. Stein, *Periodic Macroporous Hydroxyapatite-Containing Calcium Phosphates.* Chemistry of Materials, 2002. **14**(8): p. 3326-3331.
23. Yan, H., et al., *In Vitro Hydroxycarbonate Apatite Mineralization of CaO-SiO_2 Sol-Gel Glasses with a Three-Dimensionally Ordered Macroporous Structure.* Chemistry of Materials, 2001. **13**(4): p. 1374-1382.
24. Zhang, K., N.R. Washburn, and C.G. Simon Jr, *Cytotoxicity of three-dimensionally ordered macroporous sol–gel bioactive glass (3DOM-BG).* Biomaterials, 2005. **26**(22): p. 4532-4539.
25. Boonyang, U., F. Li, and A. Stein, *Hierarchical Structures and Shaped Particles of Bioactive Glass and Its In Vitro Bioactivity.* Journal of Nanomaterials, 2013.
26. Tse, A.S., Z. Wu, and S.A. Asher, *Synthesis of Dyed Monodisperse Poly(methyl methacrylate) Colloids for the Preparation of Submicron Periodic Light-Absorbing Arrays.* Macromolecules, 1995. **28**(19): p. 6533-6538.
27. Gu, Z.-Z., et al., *Rapid synthesis of monodisperse polymer spheres for self-assembled photonic crystals.* Colloids and Surfaces A: Physicochemical and Engineering Aspects, 2007. **302**(1-3): p. 312-319.
28. Li, J.Q. and R. Salovey, *"Continuous" emulsifier-free emulsion polymerization for the synthesis of monodisperse polymeric latex particles.* Journal of Polymer Science Part A: Polymer Chemistry, 2000. **38**(17): p. 3181-3187.

29. Kiatkamjornwong, S. and C. Kongsupapsiri, *Control of monodisperse particle size of styrenic–acrylate copolymers in dispersion copolymerization.* Polymer International, 2000. **49**(11): p. 1395-1408.
30. Epifani, M., et al., *Sol–Gel Processing and Characterization of Pure and Metal-Doped SnO2 Thin Films.* Journal of the American Ceramic Society, 2001. **84**(1): p. 48-54.
31. Zhong, Z., et al., *Preparation of Mesoscale Hollow Spheres of TiO2 and SnO2 by Templating Against Crystalline Arrays of Polystyrene Beads.* Advanced Materials, 2000. **12**(3): p. 206-209.
32. Schroden, R.C., et al., *Optical Properties of Inverse Opal Photonic Crystals.* Chemistry of Materials, 2002. **14**(8): p. 3305-3315.
33. Narasaraju, T.S.B. and D.E. Phebe, *Some physico-chemical aspects of hydroxylapatite.* Journal of Materials Science, 1996. **31**(1): p. 1-21.
34. Leroy, N. and E. Bres, *Structure and substitutions in fluorapatite.* Eur. Cell. Mater., 2001. **2**: p. 36-48.
35. Kuriakose, T.A., et al., *Synthesis of stoichiometric nano crystalline hydroxyapatite by ethanol-based sol–gel technique at low temperature.* Journal of Crystal Growth, 2004. **263**(1–4): p. 517-523.
36. Han, Y., et al., *Synthesis and sintering of nanocrystalline hydroxyapatite powders by citric acid sol-gel combustion method.* Mater. Res. Bull., 2004. **39**(1): p. 25-32.
37. Ruban Kumar, A. and S. Kalainathan, *Sol–gel synthesis of nanostructured hydroxyapatite powder in presence of polyethylene glycol.* Physica B: Condensed Matter, 2010. **405**(13): p. 2799-2802.
38. Fang, L., Y. Leng, and P. Gao, *Processing of hydroxyapatite reinforced ultrahigh molecular weight polyethylene for biomedical applications.* Biomaterials, 2005. **26**(17): p. 3471-3478.
39. Zheng, W., et al., *Adsorption of Cd(II) and Cu(II) from aqueous solution by carbonate hydroxylapatite derived from eggshell waste.* Journal of Hazardous Materials, 2007. **147**(1–2): p. 534-539.
40. Liao, D., et al., *Removal of lead(II) from aqueous solutions using carbonate hydroxyapatite extracted from eggshell waste.* Journal of Hazardous Materials, 2010. **177**(1–3): p. 126-130.

41. Andersson, J., et al., *Sol–gel synthesis of a multifunctional, hierarchically porous silica/apatite composite.* Biomaterials, 2005. **26**(34): p. 6827-6835.
42. Poh, C.K., et al., *In vitro characterizations of mesoporous hydroxyapatite as a controlled release delivery device for VEGF in orthopedic applications.* Journal of Biomedical Materials Research Part A, 2012: p. n/a-n/a.
43. Yuan, Y., et al., *Size-mediated cytotoxicity and apoptosis of hydroxyapatite nanoparticles in human hepatoma HepG2 cells.* Biomaterials, 2010. **31**(4): p. 730-740.
44. Jiang, M., et al., *Fe^{2+}/Fe^{3+} substitution in hydroxyapatite: Theory and experiment.* Physical Review B, 2002. **66**(22): p. 224107.
45. Srinivasan, M., C. Ferraris, and T. White, *Cadmium and Lead Ion Capture with Three Dimensionally Ordered Macroporous Hydroxyapatite.* Environmental Science & Technology, 2006. **40**(22): p. 7054-7059.
46. Zhang, K., et al., *Effects of materials parameters on mineralization and degradation of sol-gel bioactive glasses with 3D-ordered macroporous structures.* Journal of Biomedical Materials Research Part A, 2003. **66A**(4): p. 860-869.
47. Patel, M., R. Tuckerman, and Q. Dong, *A Pitfall of the 3-(4,5-dimethylthiazol-2-yl)-5(3-carboxymethonyphenol)-2-(4-sulfophenyl)-2H-tetrazolium (MTS) Assay due to Evaporation in wells on the Edge of a 96 well Plate.* Biotechnology Letters, 2005. **27**(11): p. 805-808.
48. Chen, C.S., et al., *Cell shape provides global control of focal adhesion assembly.* Biochemical and Biophysical Research Communications, 2003. **307**(2): p. 355-361.
49. Kokubo, T. and H. Takadama, *How useful is SBF in predicting in vivo bone bioactivity?* Biomaterials, 2006. **27**(15): p. 2907-2915.
50. Li, Y., et al., *Synthesis and cytocompatibility of manganese (II) and iron (III) substituted hydroxyapatite nanoparticles.* Journal of Materials Science, 2012. **47**(2): p. 754-763.
51. Bakan, F., O. Laçin, and H. Sarac, *A novel low temperature sol–gel synthesis process for thermally stable nano crystalline hydroxyapatite.* Powder Technology, 2013. **233**: p. 295-302.
52. Liu, D.-M., T. Troczynski, and W.J. Tseng, *Aging effect on the phase evolution of water-based sol–gel hydroxyapatite.* Biomaterials, 2002. **23**(4): p. 1227-1236.

53. Sun, R., Y. Lu, and K. Chen, *Preparation and characterization of hollow hydroxyapatite microspheres by spray drying method.* Materials Science and Engineering: C, 2009. **29**(4): p. 1088-1092.

54. Wang, H., et al., *Preparation of irregular mesoporous hydroxyapatite.* Materials Research Bulletin, 2008. **43**(6): p. 1607-1614.

55. Tseng, C.-L., et al., *Development of a dual-functional Pt–Fe-HAP magnetic nanoparticles application for chemo-hyperthermia treatment of cancer.* Ceramics International, 2014. **40**(4): p. 5117-5127.

Output (Acknowledge the Thailand Research Fund)

Under preparation process.